Development and experimental validation of a low-cost CMOS based spectrometer for optical and fluorescence applications

J. E Moreno Araujo[a] and C. A Hernández Gutiérrez[b]

[a]*Tecnológico Nacional de México, Instituto Tecnológico de Tuxtla Gutiérrez, Optomechatronics Group.*
[b] *Electrical Engineering Department, CINVESTAV-IPN, México City, México.*

Received 3 June 2025; accepted 9 October 2025

This work presents the design, construction, and experimental validation of a low-cost CMOS-based spectrometer built using a 3D-printed structure, a general-purpose webcam, and a low-cost diffraction grating. The system was calibrated using LED light sources and validated against a commercial Ocean HR4000CG-UV-NIR spectrometer. Results show that the CMOS-based spectrometer achieves wavelength detection accuracy within ± 7 nm and is capable of resolving emission spectra with 1 nm resolution spacing in the visible range (440-620 nm). The device was also applied to measure fluorescence in vitamin-enriched beverages and to analyze the absorbance properties of colored filters, demonstrating its utility in both chemical and optoelectronic applications. These findings confirm the feasibility of implementing low-cost spectroscopic tools for educational and scientific use.

Keywords: Spectrometer; diffraction grating; LEDs.

DOI: https://doi.org/10.31349/RevMexFis.72.020901

1. Introduction

The spectrometer is an optical instrument commonly employed to measure the wavelength and intensity of light sources. Its importance spans various scientific and technological fields, such as disinfection, where it is used to determine the optimal emission wavelength for pathogen inactivation [1-3]; biology, where it detects substances like chlorophyll, DNA, and water pollutants [4,5]; chemistry, for analyzing absorption spectra of diverse substances [1,6]; and optoelectronics, to study the emission wavelengths and stability of different light sources [1-3,7-9]. The literature highlights that spectrometer is an essential characterization instrument, and due to their high cost, they are unaffordable for many universities. Consequently, the development of low-cost spectrometers has become a significant research area for optical instrumentation specialists and engineers. Additionally, the literature indicates that spectrometer manufacturing typically involves three primary components: a CMOS sensor, a light dispersion element (such as diffraction gratings or refractive prisms) positioned at a precise angle relative to the sensor, and supplementary optical elements like collimation lenses or mirrors to minimize optical aberrations [7-9]. Light dispersion in a spectrometer occurs through a diffraction grating, typically a glass or plastic element containing numerous finely spaced lines per millimeter. When a beam of light passes through this grating, each small spacing between adjacent lines acts as a distinct coherent source. These sources emit light of identical wavelengths, producing diffracted beams that appear at specific and predictable positions on a detection screen. This diffraction phenomenon is mathematically described by the diffraction grating functions in Eq. (1):

$$d(\sin\alpha - \sin\beta) = m\lambda, \tag{1}$$

or

$$\sin\alpha - \sin\beta = Nm\lambda, \tag{2}$$

where, d space between the lines (slits) (grating period), N number of lines per mm (groove density), m order of diffraction ($m = 0, \pm 1, \pm 2$,...) and λ wavelength of the beam [10-13]. In this context, increasing the groove density (lines per millimeter) of the diffraction grating results in a decrease of the maximum achievable wavelength [14].

In the work of E. Herrera *et al.*, a low-cost spectrometer was built to measure the emission spectrum of smartphone camera lamps and LASER pointers. They demonstrated that the hardware achieved similar results in wavelength measurements than visible commercial spectrometers [7]. The state of the art indicates that the manufacturing of the device requires a specific calibration, Mattis Osterheider *et al.* also built a DIY spectrometer. They employed a mercury lamp for calibration to observe the standard emissions of this lamp ($\lambda : 557$ nm, $\lambda : 546$ nm, $\lambda : 536$ nm and $\lambda : 405$ nm) [15]. A. R. Castellanos et al. also built a low-cost spectrometer and reported that they employed mercury, neon, hydrogen, and helium lamps to calibrate their hardware. They obtained a 2% standard deviation in the results comparing their hardware with a commercial spectrometer [8]. However, there are alternative light sources to calibrate the hardware. In the work of Pradip Gatkine *et al.* they employed specific calibration LASER pointers ($\lambda : 645$ nm "red" and $\lambda : 532$ nm "green") instead of discrete lamps [9]. In this work, they also employed a general purpose software for webcam-based spectrometers developed by Theremino, to obtain the plots of the observed spectrum [16]. Wenderson R. F. Silva *et al.* reported on spectrometers to build a device capable of measuring emission, absorption, and fluorescence. They reported the fluorescence and concentration of quinine in tonic

water [4]. All previous works emphasize device calibration settings, employing spectrum references of different emitting devices. This work reports the wavelength detection accuracy, employing scanning electron microscopy (SEM) for the grid structural characterization combined with reference light sources such as LEDs and LASER to calibrate the low cost hardware. We designed the hardware to ensure and preserve the alignment of the optical elements after calibration, and developed a Python software to perform spectrometry experiments. This software measures the fluorescence of different substances (B vitamins derivatives and Quinine hydrochloride) in commercial beverages and approximates substance concentrations based on their signal intensity. We also employed the CMOS-based hardware to measure the wavelength absorption of broad-spectrum white light when it passes through different color filters (CYM cube), in Fig. 1f) is shown the experimental setup utilized to measure the light transmitted spectrum when white light passes through the color filters [27-29].

2. Materials and methods

This section describes the materials, the construction details, and the calibration of the spectrometer hardware. The CMOS-based spectrometer was constructed using a Logitech C270 webcam as the CMOS detector, with a sensor size of 3.58×2.02 mm, pixel dimensions of 2.8 μm (square), and a resolution of 1280×720 pixels. A diffraction grating with a groove density of 1000 lines/mm was selected as the dispersive element, as this specification is commonly used for scattering light within the visible (VIS) spectrum. This type of optical component is widely available through online retailers at an affordable price of approximately $2 USD, making it ideal for educational purposes and accessible to students and universities. The mechanical structure of the spectrometer was designed using SolidWorks CAD software and fabricated with a FLASHFORGE Guider IIs 3D printer. Polylactic Acid (PLA) was selected as the printing material due

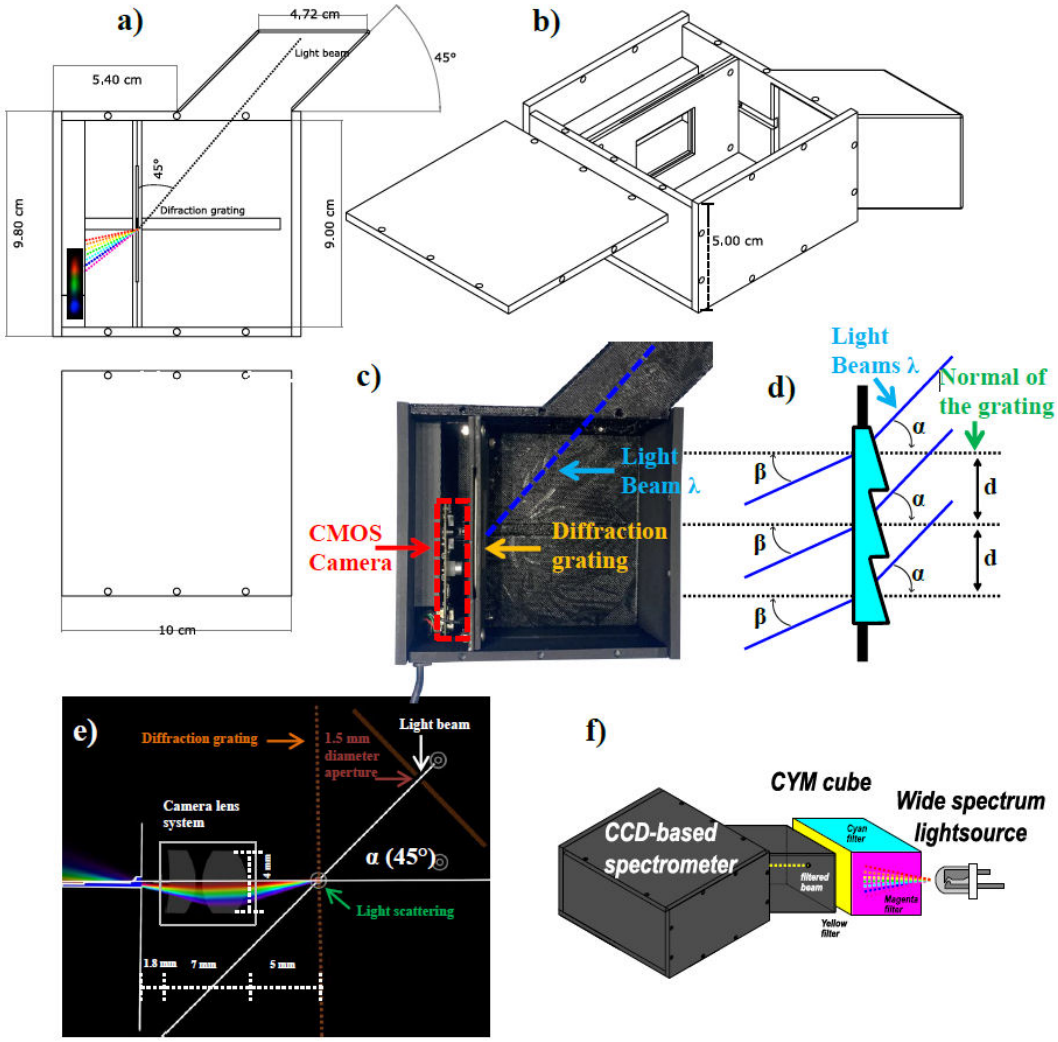

FIGURE 1. a) Superior view of CMOS-based spectrometer, b) Isometric view of the device, c) Final 3D printed hardware, and d) Optical scheme of the diffraction grating model, e) Optical Diagram of the CMOS-based spectrometer and f) Experimental setup for absorbance measurements.

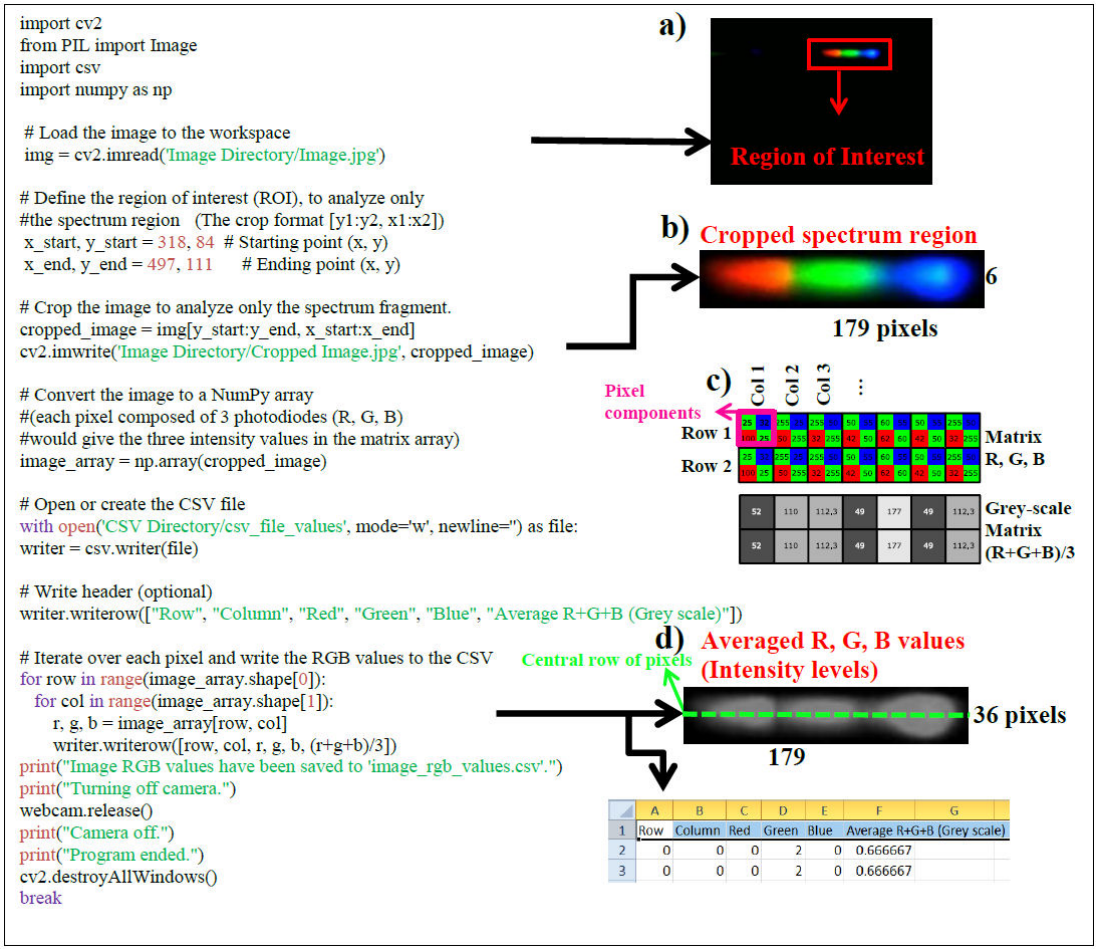

FIGURE 2. a) Image capture of the spectrum, b) Isolation of the Region of Interest (ROI), c) RGB components of Bayer matrix and d) Horizontal cross-section of the spectrum.

to its ease of use and dimensional stability. The structure ensures that all optical components remain fixed, minimizing mechanical shifts that could lead to hardware misalignment; the optical input of the CMOS-based spectrometer consists of a 1.5 mm diameter aperture located on an arm extending from the main body of the device, where only the light from the source is addressed. Detailed views and dimensions of the final hardware and its optical scheme are illustrated in Figs. 1a) - 1d). Figure 1e) presents a diagram of the optical components of the CMOS-based spectrometer. The "Ray Optics Simulator" was employed using distance measurements and a rough estimation of the camera lens geometry. To verify the optical quality of the manufacturing process for the diffraction grating, a morphological characterization was performed using Scanning Electron Microscopy (SEM) at an acceleration voltage of 1 kV, assessing the type of structure employed in the optical scattering hardware and its characteristics, such as width, shape, spacing, and periodicity of the scattering structures. The angle at which the incident light beam enters the spectrometer is governed primarily by the diffraction grating's physical characteristics namely its groove density and blaze angle. These parameters, which define the angular dispersion and spectral efficiency of the grating, are typically specified by the manufacturer [10,11]. Accurate alignment of the light source with respect to the grating is essential, as it directly influences the resolution and position of the projected spectrum on the detector. The spectrometer calibration and resolution assessment were conducted by analyzing the spectral emissions of six ultrabright LED light sources of Chanzon manufacturing company, with nominal peak wavelengths at 461 nm, 452 + 534 nm (dual-peak), 605 nm, 630 nm, 450 nm + 627 nm (dual-peak), and 593 nm. The LEDs also have, 3 mm lens size with a viewing angle of 30° and 20 mA of current consumption. As a reference, an Ocean Optics HR4000CG-UV-NIR spectrometer was used, offering a high spectral resolution of 0.250 nm and covering a broad wavelength range from 195 nm to 1132 nm, encompassing the UV to near-infrared regions. Finally, for the signal processing, a custom Python algorithm was developed to analyze and convert CMOS-detected scattered light intensities into emission spectra. The software exports intensity values (0 to 255 in arbitrary units) and a wavelength spacing of 1 nm in a CSV file suitable for further analysis in data-processing software; a commented version of this code is shown in Fig. 2.

2.1. Code explanation

The algorithm acquires the spectral image and processes it to generate a .CSV file, enabling the data to be plotted as measurement graphs. To begin, the incident light beam is dispersed by the diffraction element into its constituent wavelengths, producing a spectral distribution that is projected and recorded by the CMOS camera. The process begins by capturing a complete image. In cases where the spectrum does not entirely fit within the frame, as in Fig. 2a) where it appears in the upper-right corner, the image would need to be cropped to isolate the spectrum of the rest of the imagen, calling this secondary process a Region of Interest (ROI), highlighted in red in Fig. 2b). Isolating the spectrum from the rest of image enables the algorithm to process only the relevant region while excluding dark areas with no information, thereby reducing computational workflow and processing time. Every pixel of the ROI image is composed by 3 different (RGB) values corresponding to Red, Green, and Blue elements as shown in the Bayer matrix represented in the Fig. 2c). To quantify light intensity in one pixel, the algorithm calculates the mean of its R, G, and B components. This process reduces the color image into a grayscale suitable for further spectral analysis [38]. This conversion reduces 3 values (R,G,B) per pixel into a single intensity value per pixel, which indicates the light intensity in arbitrary units ranging from 0 to 255. The processed data is then exported by the algorithm into a .CSV file, which includes the row and column corresponding to R, G, B and Intensity values of each pixel that is in the ROI. Spectrometers by defect export this .CSV as data file to construct emission curves employing data processing software; to obtain the graph is necessary to plot in the y axis the intensity values of one row of pixels of the image representing a horizontal cross-section of the spectrum represented by the green line in the Fig. 2d) [30].

2.2. Calibration of the emission signal

The calibration process is the final step to build the CMOS-based spectrometer. However, in the spectrometer operation, many variables make calibration an empirical task [30]. Spectrometer calibration is commonly performed utilizing standard emitting sources, such as calibration LEDs or characteristic line-emitting lamps (*e.g.*, mercury-argon), to generate a calibration curve for the detector [30-32]. For the CMOS-based hardware, the process began with preliminary measurements of red and blue LED light sources using the commercial Ocean Optics HR4000CG-UV-NIR spectrometer, to identify their precise emission peaks ($\lambda_{\text{blue}} \approx 461$ nm and $\lambda_{\text{red}} \approx 630$ nm), which lie near the limit range of the diffraction grating. These initial references are recorded by the CMOS-based, the emission signal peaks measured by both instruments, the CMOS-based and the Ocean commercial spectrometer were overlapped to match the signal peaks [33], in this process, the diffraction grating was heuristically adjusted relative to the sensor (closer or further) to minimize discrepancies between the overlapped signal peaks, the final distances and dimensions of the optical elements are shown in the Fig. 1e). Once the spectrometer limit range was aligned, additional LEDs ($\lambda_{\text{yellow}} \approx 593$ nm, and $\lambda_{\text{orange}} \approx 605$ nm) were measured to compare their emission peaks across both devices [34]. Calibration was ultimately validated by measuring and overlapping the spectrum of a white LED light source, which provides a broad emission spectrum and two signal peaks ($\lambda_{\text{blue}} \approx 452$ nm, $\lambda_{\text{green}} \approx 534$ nm) [35,37], and by using standard sources such as tonic water fluorescence, which exhibits a characteristic peak at 444 nm as reported in the literature [21,22].

2.3. Fluorescence experiment

The CMOS-based spectrometer was employed to capture fluorescence spectra of a UV-A LED lamp with an emission wavelength of 405 nm as the excitation source. Fluorescence measurements were performed on samples consisting of 1000 μL each of commercial energy soda (containing Vitamin B3: 5.1 mg, Vitamin B2: 720 μg, Vitamin B6: 850 μg, and Vitamin B12: 2.5 μg), vitamin-enriched water (Vitamin B3: 1.65 mg, Vitamin B5: 0.80 mg, Vitamin B6: 165 μg, Vitamin B12: 0.5 μg, and Vitamin C: 25 mg), and tonic water containing quinine hydrochloride. Distilled water was employed to reduce the concentration of commercial energy soda at the bias concentrations (1, 0.5, 0.25, 0.125) to achieve the fluorescence signal intensity analysis in the function of energy soda concentration.

2.4. Absorbance experiment

The CMOS-based spectrometer was employed to measure the absorbance characteristics of coatings deposited on the faces of a CYM (Cyan, Yellow, Magenta) transmission filter cube. A broad-spectrum LED emitting in the wavelength range of 400 nm to 635 nm was utilized as the light source to identify and analyze the wavelengths absorbed by each filter coating.

3. Experimental results

3.1. Diffraction grating characterization

The characterization of the diffraction grating was performed to know the morphology details of the diffraction grating, such as the kind of structure employed to scatter light and the exact separation of these structures in the grating. SEM analysis Figs. 3a) and 3b) show that the scattering device is built employing parallel lines with an approximate width of 500 nm and a separation of 1 μm between structures. The periodic separation and the size of the lines help to determine the wavelength range in which the light is decomposed when passing through the device, making the device suitable for scattering light in the region between 440 nm and 625 nm [14]. Figure 3c) also revealed the presence of defects with

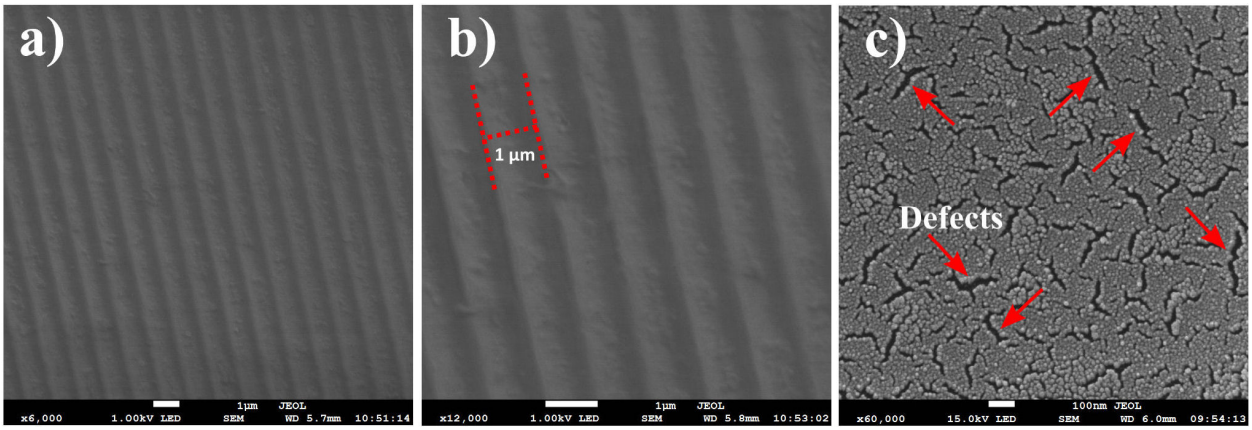

FIGURE 3. a) SEM surface analysis x6,000 magnification, b) SEM surface analysis x12,000 magnification, c) SEM posterior analysis x60,000 magnification.

average size of 150 nm on the back surface of the transmission grating, fortunately the defects size does not coincide with incident wavelengths and does not cause unintended scattering of light in the VIS range [13], defects could cause unwanted scattering in shorter wavelengths because each imperfection would act as a coherent light source [17-20].

3.2. Spectral characterization of LED Light sources

Figures 4a) - 4h) presents a comparative analysis of the spectral measurements obtained from LED light sources using both the OCEAN HR4000CG-UV-NIR reference spectrometer and the CMOS-based hardware developed in this work. The comparison is organized into three spectral regions: violet-green (400-550 nm), green-red (550-675 nm), and the full visible range (400-750 nm), the latter used for broadband sources such as white and violet LEDs. In Figs. 4a) and 4b), the CMOS-based hardware shows broader full width at half maximum (FWHM) values for the blue and violet LED emission curves compared to those obtained with the commercial OCEAN spectrometer. This effect is attributed to the lower optical quality of the components used in the developed low-cost CMOS-based setup, which limits its ability to resolve finer spectral details in the short-wavelength region. Conversely, in Fig. 4c), 4d), and 4e), the CMOS-based hardware demonstrates improved FWHM resolution for the yellow (593.75 nm), orange (611.02 nm), and red (623.97 nm) LEDs, indicating better performance in the longer-wavelength region compared to the blue range. These results confirm that the CMOS-based system is capable of measuring electroluminescence with a wavelength resolution of ± 1 nm and achieving an accuracy of ± 7 nm when compared to the commercial OCEAN spectrometer. However, an inaccurate measurement was observed in the red emission component (615 nm) of the dual-emission violet LED, which exhibited an unexpected attenuation of the red signal, as highlighted in the pink region of Fig. 4f). This discrepancy is attributed to an IR optical filter integrated into the CMOS camera, commonly employed to reduce IR noise during low-light conditions, absorbing red-IR wavelengths and limiting the ability of the CMOS-based spectrometer to read emissions of larger wavelengths to 623 nm accurately. In Fig. 4h) and i), an additional discrepancy in the emissions of UV light sources is shown, which arises from the limitations of the diffraction grating. In the commercial spectrometer, a 12 nm separation between the emission peaks of the UV-A LASER and the UV-A LED. However, the spectrum produced by the CMOS-based hardware shows 1 nm separation between peak signals, indicating that the hardware is unreliable for UV analysis. Furthermore, the measurements obtained from the CMOS-based hardware are shifted further into the UV spectrum, displaying values of 385 nm and 386 nm rather than the expected 417 nm and 405 nm.

TABLE I. Comparison of LED light sources measurements.

Device	Forward Voltage	Ocean HR4000CG -UV-NIR	CMOS-Based Diffraction grating	FWHM Ocean HR4000CG-UV-NIR	FWHM CMOS-Based Diffraction grating
LED "RED"	1.902 V	630.82 nm	623.97 nm	13.13 nm	14.29 nm
LED "YELLOW"	2.127 V	593 nm	593.75 nm	18.15 nm	16.55 nm
LED "VIOLET"	3.123 V	450 nm + 627 nm	442.66 nm + 615.34 nm	17.87 nm, 85 nm	30.3 nm, 61 nm
LED "ORANGE"	2.012 V	605 nm	611.02 nm	14.83 nm	22.44 nm
LED "WHITE"	3.189 V	452 nm + 534 nm	448.41 nm + 533.319 nm	16.8 nm, 111.3 nm	21.67 nm, 101.7 nm
LED "BLUE"	2.610 V	461 nm	459.93 nm	21.07 nm	33.04 nm

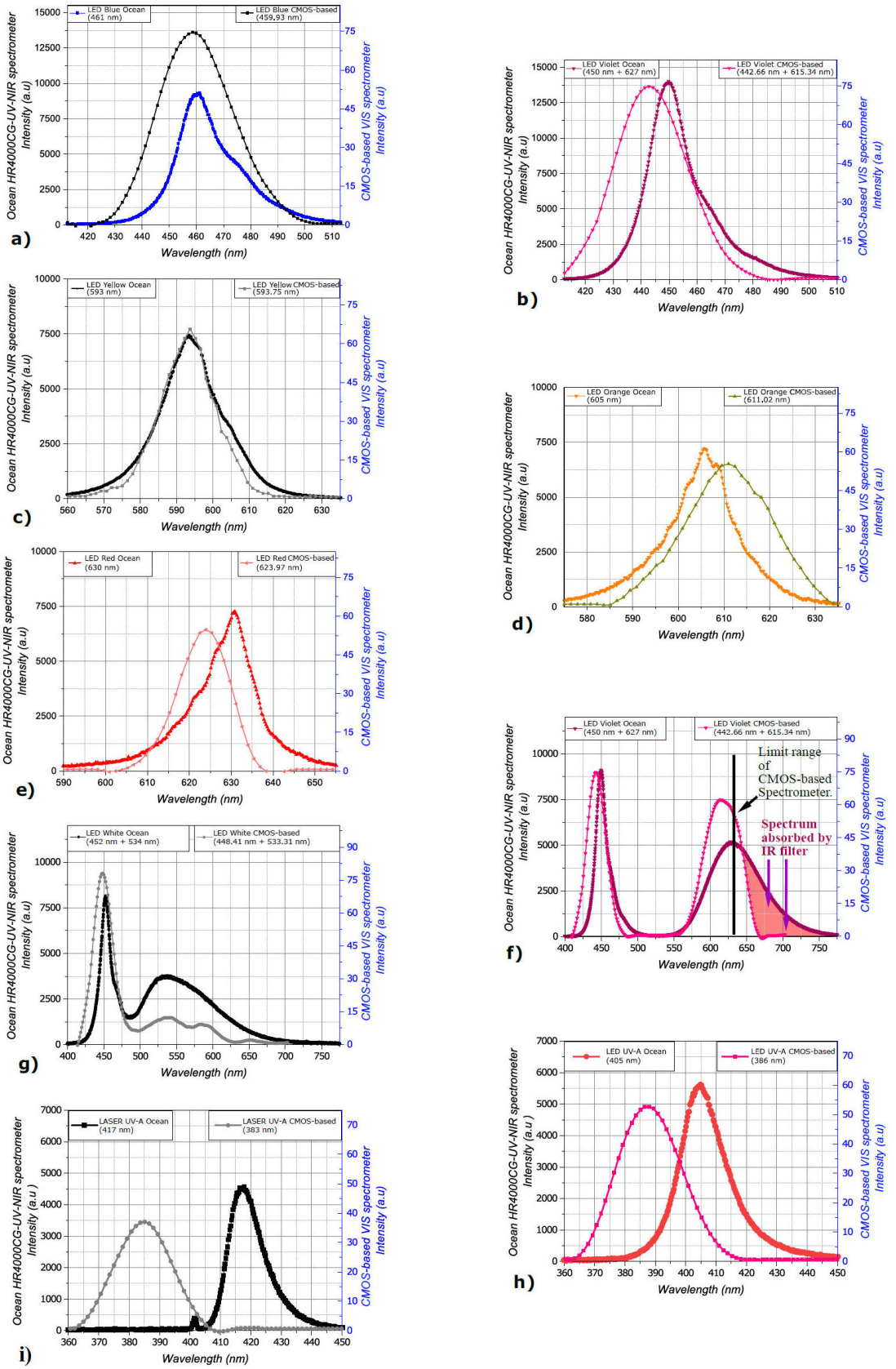

FIGURE 4. a) - h) Comparison of LED emission wavelengths obtained using the commercial spectrometer and the CMOS-based hardware. Subfigures show measurements in the violet a), blue b), visible c), d), e), wide-spectrum emission f), g), and UV h) ranges. i). UV-A laser emission wavelengths are compared using both the commercial spectrometer and the CMOS-based hardware.

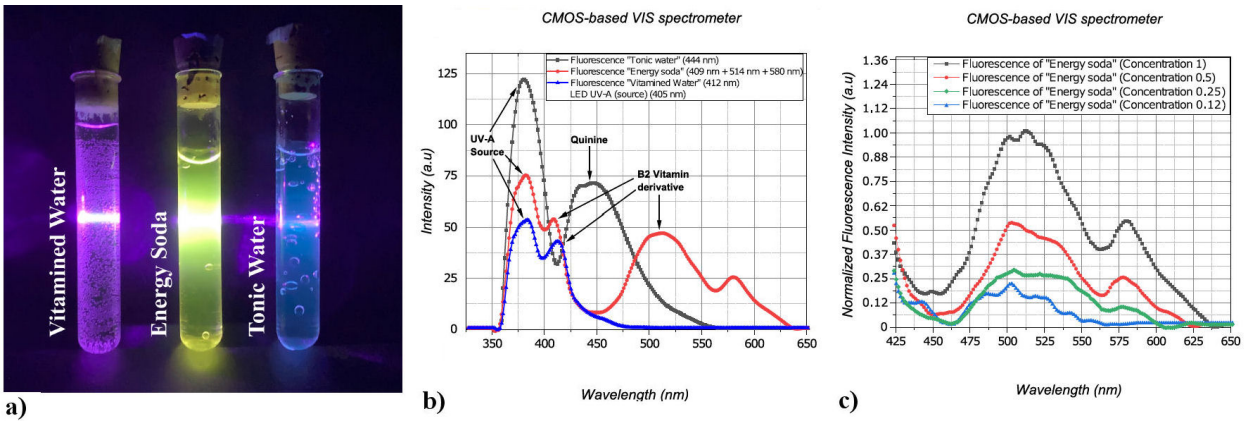

FIGURE 5. a) Fluorescence emission of samples employing CMOS-based spectrometer and UV-A LED light source, b) Fluorescence spectrum measurements of the samples (Tonic water, Energy soda, Vitamined Water), c) Normalized Fluorescence Intensity of Energy soda as function of bias concentration: 1, 0.5, 0.25, 0.125.

Table I shows a comparative analysis of the prototype CMOS-based spectrometer against the commercial Ocean HR4000CG-UV-NIR spectrometer, focusing on wavelength accuracy and the Full Width Half Maximum (FWHM) parameter. The prototype demonstrated good wavelength accuracy, especially at intermediate wavelengths (*e.g.*, yellow LED with only 0.75 nm deviation). However, greater discrepancies were evident at shorter wavelengths (violet and blue LEDs), likely due to the limit range of diffraction grating, which causes unwanted scattering in shorter wavelengths. The prototype also exhibited a slightly lower spectral resolution compared to the commercial device, particularly noticeable at shorter wavelengths (below 500 nm). These findings indicate that, although the prototype performs adequately for general optoelectronic purposes, further improvements in diffraction grating quality are necessary to enhance its accuracy and resolution at shorter wavelengths.

3.3. Fluorescence results

Another application of this work is the fluorescence. Figure 5a) illustrates the fluorescence of commercial tonic water, vitamin water, and energy soda, employing the CMOS-based spectrometer as measurement instrument and a UV-A lamp (405 nm) as excitation light source. Figure 5b) shows that the tonic water sample exhibits a fluorescence signal peak at 444 nm, which generates a glowing blue fluorescent emission attributed to the presence of quinine hydrochloride, the compound responsible for the fluorescence at this wavelength [21,22]. The spectrum does not indicate the presence of other fluorescent substances in the tonic water, such as vitamins or phenolic compounds. Figure 5b) also reveals that the vitamins added to the vitamin water and energy soda samples produce a peak signal in 409 nm, likely due to the presence of derivatives of B vitamins in both liquids [23]. In this plot is also shown that the energy soda sample fluorescence, radiates three peak signals at 409 nm, 514 nm, and 580 nm, which may be attributed to riboflavin (vitamin B2) and other B vitamin derivatives, which produce an intense fluorescent glow in the green - yellow region [23-25] as it is shown in the Fig. 5a).

In Fig. 5c), the Normalized Fluorescence Intensity signal of the energy soda sample as a function of different concentration biases is observed. The CMOS-based hardware accurately measured half of the fluorescence intensity of the "Energy Soda" when its concentration was reduced to half of the initial concentration. Subsequently, it precisely measured a quarter and an eighth of the fluorescence intensities when the concentration was reduced to a quarter and subsequently an eighth of the initial concentrations, thereby indicating a proportional relationship between the fluorescence intensity (in a.u) and the concentration of the sample. This feature is relevant where the fluorescence light intensity could be taken as a parameter to indicate the concentration of one substance dissolved in the liquid [6,26].

3.4. Absorbance results

In Fig. 6a) is shown that the yellow coating absorbed the blue component (435 nm) from the wide spectrum source, exhibiting the same intensity of the transmitted blue component and the yellow-green components. This absorption transforms the beam in a yellow-green color as shown in the photo on the plot. In Fig. 6b), it is demonstrated that Cyan coating absorbed the range of orange - red components (564 - 623 nm), letting the filter transmits just the blue-green-yellow components, coloring the beam in a sky-blue color, as shown in the photo on the plot. In Fig. 6c) is shown that magenta coating absorbed the range of blue-green-yellow colors (474 - 569 nm), letting the filter to transmit the outer limits of the wide spectrum source LED, color violet (433 nm) and red (600 nm) components, the absorption let the filter to color the beam in violet color as it is shown in the photo on the plot. This emission measurements exhibit a similar behavior to the Violet LED described in Sec. 3.2.

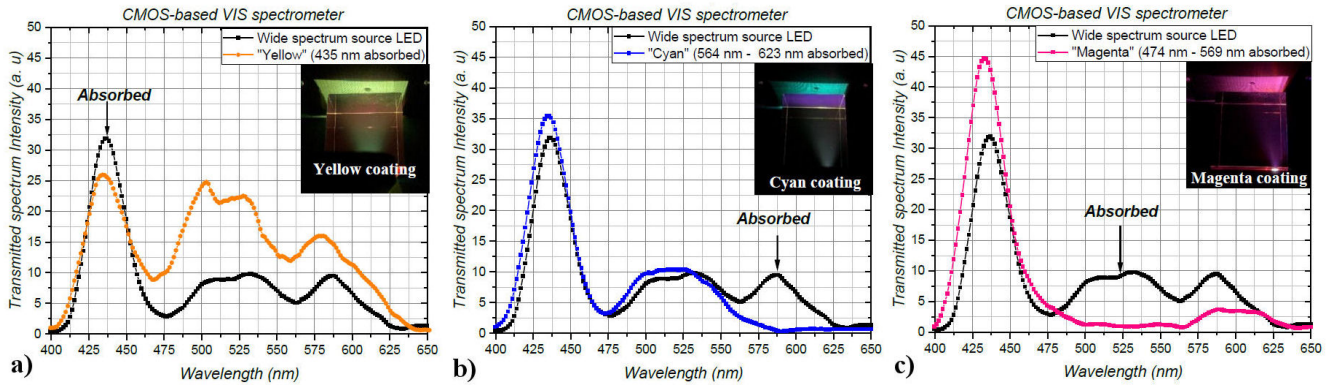

FIGURE 6. a) Transmitted spectrum intensity through the yellow filter, b) Transmitted spectrum intensity through the cyan filter, and c) Transmitted spectrum intensity through the magenta filter.

4. Conclusions

This paper reported the overview of the methodology for the design and development of a low-cost CMOS-based spectrometer, capable of performing basic spectroscopy experiments such as fluorescence, absorbance, substance concentration and measurement of wavelength light sources emission. The hardware required low-cost materials like 3D PLA printed pieces, a general-purpose diffraction grating, and a CMOS camera, which required approximately 15 USD. The hardware allows obtaining wavelength measurement accuracy of ± 7 nm. In addition, the system also measured indirect parameters such as the substance proportion in the function of its fluorescence intensity. The accuracy of the CMOS-based spectrometer is directly influenced by the quality of the individual components, particularly the diffraction grating, which had an accurate performance in the VIS region (440 - 620 nm), but an critical error increase in the Blue-Violet region, affected by the wavelength scattering range of the hardware. Another improvement of the CMOS-based hardware is employing a camera with a larger image resolution and smaller pixel size to obtain more precise emission curves, lowering the 1 nm wavelength spacing. Therefore, a comprehensive characterization of the individual components such as Scanning Electron Microscope (SEM) images of the diffraction grating and the precise emission wavelength of light sources were employed to understand these physical limitations of the diffraction grating in scattering light, in consequence the experiments performed in the UV region with LED-LASER light sources present higher error rates and inaccuracies of spectrum measurements due to those physical limitations of the diffraction grating to scatter UV-Violet-Blue wavelengths. Red detection issues were observed in the hardware, which are attributed to the presence of an infrared (IR) filter deposited on the CMOS sensor to reduce noise from light in the red-IR spectrum. Despite this, the low-cost system is capable of performing scientific experiments with sufficient accuracy for chemical, optoelectronic, and biological applications. It is essential to consider that the hardware is compact and robust, and incorporates a Python algorithm to obtain the spectrum data, similar to commercial hardware. A further advantage of this hardware is that it can be taken apart to adapt special optical instrumentation to perform specific experimental setups.

Acknowledgments

The authors are grateful to the Tecnológico Nacional de México for their support to develop the research.

Funding

This work was supported by the SECIHTI by its National Scholarship Program.

1. J. E. M. *et al.*, Design strategies based on UV-C LED characterization to enhance Escherichia coli inactivation, *Journal of Water Process Engineering* **62** (2024) 105423, https://doi.org/10.1016/j.jwpe.2024.105423
2. C. L. *et al.*, Optimized parameters for effective SARSCoV-2 inactivation using UVC-LED at 275 nm, *Scientific Reports* **12** (2022), https://doi.org/10.1038/s41598-022-20813-4
3. Y. G. *et al.*, UV-LED disinfection of Coronavirus: Wavelength effect, *Journal of Photochemistry and Photobiology B: Biology* **212** (2020), https://doi.org/10.1016/j.jphotobiol.2020.112044
4. W. R. F. S. *et al.*, Multifunctional Webcam Spectrophotometer for Performing Analytical Determination and Measurements of Emission, Absorption, and Fluorescence Spectra, *J. Chem. Educ.* **98** (2021) 1442, https://doi.org/10.1021/acs.jchemed.0c01085
5. M. S. *et al.*, Ultraviolet absorption of contaminants in water, *Scientific Reports* **11** (2021), https://doi.org/10.1038/s41598-021-83322-w

6. Ángel Herráez, Texto Ilustrado e interactivo de Biología Molecular e Ingeniería Genética / Estructura y función del material genético, 2nd ed. (Elsevier España, 2012), p. 17.
7. E. H. *et al*., Construction of visible spectrophotometer for optical spectroscopy demonstrations, *Opt. Pura Apl.* **57** (2024) 51174, https://doi.org/10.7149/OPA.57.2.51174
8. A. R. R. C. *et al*., Quantitative characterization of light through a homemade spectrometer: A STEM project-based learning activity, *Rev. Mex. Fis. E* **22** (2025) 010205, https://doi.org/10.31349/RevMexFisE.22.010205
9. P. G. *et al*., A Do-it-yourself Spectrograph Kit for Educational Outreach in Optics and Photonics, *Proc. of SPIE* **10741** (2018) 2321640, https://doi.org/10.1117/12.2321640
10. E. Hetch., Optics / Diffraction / 10.2.8 The Diffraction Grating, 5th ed. (Pearson Education, ISBN 10: 1-292-09693-4, 2017), pp. 496-502.
11. D. Malacara., Óptica básica / Aplicaciones de la difracción y tomografía óptica, 3rd ed. (Fondo de Cultura Económica, ISBN 978-607-16-3215-9, 2015), pp. 297-298.
12. G. R. Harrison., The Production of Diffraction Gratings: II. The Design of Echelle Gratings and Spectrographs, *Journal of the Optical Society of America* **39** (1949) 522, https://doi.org/10.1364/JOSA.39.000522
13. T. N. W. *et al*., Scattered-light properties of diffraction gratings, *Applied Optics* **33** (1994) 4273, https://doi.org/10.1364/AO.33.004273
14. Newport, Determining the Maximum Achievable Wavelength of a Monochromator or Spectrograph, (2024), https://www.newport.com/t/determining-the-maximumachievable-wavelength-of-a-monochromator-or-spectrograph
15. M. O. *et al*., A do-it-yourself Czerny-Turner spectrometer: atomic emission, absorption, reflection and fluorescence spectroscopy in natural sciences, *Phys. Educ* **57** (2022), https://doi.org/10.1088/1361-6552/ac8a85
16. Theremino Spectrometer (2025), https://www.theremino.com/wp-content/uploads/files/Theremino_Spectrometer_Technology_ENG.pdf
17. Newport, Handling Diffraction Gratings (2024), https://www.newport.com/n/handling-diffraction-gratings
18. S. C. C.-G. *et al*., Sensing fabrication errors in diffraction gratings using high dynamic range imaging, *Optics Express* **27** (2019) 21880, https://doi.org/10.1364/OE.27.021880
19. J. S. *et al*., Analysis of the loss resulting from point defects for an etched diffraction grating demultiplexer by using the method of moments, *Journal of the Optical Society of America* **22** (2005) 1620, https://doi.org/10.1364/JOSAA.22.001620
20. C. Palmer., Diffraction Grating Handbook, 8th ed. (MKSNewport, 2020), p. 209.
21. A. H. *et al*., Fluorescence Analysis of Quinine in Commercial Tonic Waters, *Methods Protoc* **8** (2025), https://doi.org/10.3390/mps8010005
22. I. R. *et al*., A Fluorescent Mid-Air Screen, 2013 IEEE International Symposium on Multimedia (2013), https://doi.org/10.1109/ISM.2013.14
23. Y. H. *et al*., Intrinsic Fluorescence Spectra Characteristics of Vitamin B1, B2 and B6, *Proc. Of SPIE* **9795** (2015), https://doi.org/10.1117/12.2216038
24. X. L. *et al*., Ag NPs/PMMA nanocomposite as an efficient platform for fluorescence regulation of riboflavin, *Optics Express* **30** (2022) 34918, https://doi.org/10.1364/OE.470454
25. Y. Z. *et al*., Effect of the Synthetic NC-1059 Peptide on Diffusion of Riboflavin across an Intact Corneal Epithelium, Cornea, *Investigative Ophthalmology and Visual Science* **53** (2012) 2620, https://doi.org/10.1167/iovs.12-9537
26. W. Y. *et al*., A catalytic cleavage strategy for fluorometric determination of Hg(II) based on the use of a Mg(II)-dependent split DNAzyme and hairpins conjugated to gold nanoparticles, *Microchimica Acta* **185** (2018), https://doi.org/10.1007/s00604-018-2990-4
27. Y. W. *et al*., Compact characterization of liquid absorption and emission spectra using linear variable filters integrated with a CMOS imaging camera, *Scientific Reports* **6** (2016), https://doi.org/10.1038/srep29117
28. R. C. B. *et al*., Spectroscopic measurement of ignition parameters in forest fuel, Proc. SPIE 9219, *Infrared Remote Sensing and Instrumentation XXII* **92190H** (2014), https://doi.org/10.1117/12.2061167
29. W. Y. *et al*., Multiplexed Optical Imaging of Tumor-Directed Nanoparticles: A Review of Imaging Systems and Approaches, *Nanotheranostics* **1** (2017) 369, https://doi.org/10.7150/ntno.21136
30. J. James, Spectrograph design fundamentals (Cambridge University Press, ISBN 978-0-521-86463-3, 2007), pp. 168-170.
31. Y. C. S. *et al*., Accurate wavelength calibration method for compact CCD spectrometer, *Journal of the Optical Society of America A* **34** (2017) 498, https://doi.org/10.1364/JOSAA.34.000498
32. A. T. *et al*., Echelle spectrometer calibration by means of laser plasma, *Spectrochimica Acta Part B: Atomic Spectroscopy* **178** (2021), https://doi.org/10.1016/j.sab.2021.106144
33. S. P. Davis., Diffraction Grating Spectrographs (Holt, Rinehart and Wiston Inc, SBN: 03-077205-2, 1979), pp. 49-50.
34. M. A. H. *et al*., Combined "dual" absorption and fluorescence smartphone spectrometers, *Optics Letters* **40** (2015) 1737, https://doi.org/10.1364/OL.40.001737
35. K. G. *et al*., Illuminance meter calibration with a LED spectrally tunable light source, *Lighting Research and Technology* **52** (2020) 1009, https://doi.org/10.1177/1477153520905618
36. K. L. *et al*., Portable low-cost open-source wireless spectrophotometer for fast and reliable measurements, *HardwareX* **7** (2020), https://doi.org/10.1016/j.ohx.2020.e00108
37. D. C.-P. *et al*., Spectroscopy Transmittance by LED Calibration, *Sensors* **19** (2019) 13, https://doi.org/10.3390/s19132951
38. C. K. *et al*., Color-to-Grayscale: Does the Method Matter in Image Recognition?, *Plos One* **7** (2012) 1, https://doi.org/10.1371/journal.pone.0029740